JOURNAL OF THERMOPHYSICS AND HEAT TRANSFER
Vol. 13, No. 4, October–December 1999

Heat Transfer in the Melt Layer of a Simple Ablation Model

Tse-Fou Zien*
U.S. Naval Surface Warfare Center, Dahlgren, Virginia 22448-5000
and
Chin-Yi Wei†
National Cheng-Kung University, Tainan 70101, Taiwan, Republic of China

A simple mathematical model for steady aerodynamic ablation under hypersonic conditions is presented. The model consists of three regions, namely, an air boundary layer, a melt layer, and an ablating solid, and it is applied to the case of a simple ablation near the stagnation-point of a two-dimensional, circular-nosed body in hypersonic flow. An analysis of the model problem is presented, based on the formulation of similarity solutions. Appropriate boundary conditions on the interfaces are derived and applied to couple the three regions of interest of the model. Parameters characterizing different regions are identified. Particular emphasis is placed on the melt layer and its effect as a heat shield to the solid structure. Both the numerical solutions and the analytical solutions by the Kármán–Pohlhausen integral method are presented. A computational procedure is suggested for the whole coupled ablation problem, using the integral solutions, and an example of the application of the procedure is given.

Nomenclature

C = constant in the viscosity–temperature relation for air
Cp = specific heat at constant pressure
$\tilde{c}$ = constant defined in Eq. (33a)
$E(1)$ = constant defined in Eq. (54c)
F_1 = x component of velocity in melt layer; Eq. (18)
F_2 = z component of velocity in melt layer; Eq. (19)
f_1 = similarity function in the air boundary layer
G_2 = dimensionless temperature in the melt layer; Eq. (45)
g_1 = dimensionless temperature in the air boundary layer, T/Te
H_1 = total enthalpy of air in the freestream
I = function defined in Eq. (53a)
K = effective Peclet number
K_1 = constant parameter of melt layer; Eq. (24)
K_2 = constant parameter of melt layer; Eq. (29)
k = thermal conductivity
l = length scale for the air boundary layer; Eq. (67a)
M_∞ = freestream Mach number
m = dimensionless parameter; Eq. (82)
N = Newtonian flow parameter; Eq. (3)
N_m = dimensionless parameter for material properties in air and melt; Eq. (85)
Pr = Prandtl number
p = pressure
p_b = surface pressure near the stagnation-point
Q_L = latent heat of solid per unit mass
$(\dot{q}_{12})_1$ = heat flux at air–melt interface (leaving air region)
$(\dot{q}_{12})_2$ = heat flux at air–melt interface (entering melt region)
$(\dot{q}_{23})_2$ = heat flux at melt–solid interface (leaving melt region)
R = radius of circular-nosed body
R^* = nondimensional temperature at air–melt interface, T^*/Te
r = shielding factor; Eq. (55a)
$\tilde{r}$ = modified shielding factor, $(k_2^*/k_{2m})r$
T = temperature
$(\boldsymbol{u}, \boldsymbol{w})$ = velocity vector
V = characteristic normal velocity in air boundary layer; Eq. (67b)
W_m = ablation speed
$\overline{W}_m$ = dimensionless ablation speed, W_m/V
(x, z) = Cartesian coordinate system fixed on ablation front
$\tilde{x}$ = x/z^*
z^* = melt-layer thickness
$\overline{z^*}$ = dimensionless melt-layer thickness, z^*/ℓ
α_1 = profile parameter of the air boundary layer
α_2 = profile parameter of the air boundary layer
α_3 = profile parameter of the melt layer
$\tilde{\alpha}$ = effective thermal diffusivity
β_1 = inviscid velocity gradient at the stagnation-point
γ = specific heat ratio of the air
ε = (unknown) constant in the velocity at the air–melt interface
η_1 = modified similarity variable; Eq. (5)
η_2 = similarity variable in the melt layer, z/z^*
Θ = nondimensional temperature
μ = dynamic viscosity
$\bar{\mu}_2$ = average dynamic viscosity of the melt layer
ν = kinematic viscosity
$\bar{\nu}_2$ = average kinematic viscosity of the melt layer
ξ_1 = modified similarity variable; Eq. (4)
ρ = density
τ = shear stress
υ = ablation parameter, identical to $Q_L/c_3(T_m - T_i)$

Subscripts

e = conditions in the external inviscid flow
m = conditions on the ablation front
0 = conditions at the stagnation-point for inviscid flow or at the ablation front, $z = 0$
1 = conditions in the air boundary layer
2 = conditions in the melt layer
3 = conditions in the ablating solid
∞ = conditions of freestream

Superscript

$*$ = conditions at the air–melt interface

Received 4 December 1998; presented as Paper 99-0470 at the AIAA 37th Aerospace Sciences Meeting, Reno, NV, 11–14 January 1999; revision received 28 May 1999; accepted for publication 18 June 1999.

*Senior Research Scientist, Dahlgren Division, System Research and Technology Department; also Visiting Professor, Institute of Aeronautics and Astronautics, National Cheng-Kung University, Tainan 70101, Taiwan, Republic of China. Associate Fellow AIAA.
†Research Associate, Institute of Aeronautics and Astronautics.

I. Introduction

An understanding of the aerodynamic ablation phenomena is essential to the optimum design of thermal protection systems for various aerodynamic operations in ultra-high-temperature environments. Examples of such severe environments include those encountered by spacecraft during reentry into the Earth's atmosphere, reentry missiles and vertical launcher systems for missiles or space vehicles, to name only a few. However, aerodynamic ablation has long been recognized as one of the most challenging problems in aerodynamic heating. Experimentally, it is difficult to simulate the phenomena in a ground testing facility, and flight test for such a phenomenon is generally prohibitively expensive. From a theoretical standpoint, the problem is made difficult by its inherent complexities that include phase changes, moving interfaces, various physical/chemical reactions, and the strong coupling of different regions of interest.

One of the purposes of the present work is to provide some understanding of the basic fluid dynamic aspects of the phenomena by developing a mathematical model for simple aerodynamic ablation problems that are amenable to relatively simple theoretical analyses. The model should be useful for parametric studies of the basic elements of the fluid dynamics and heat transfer associated with aerodynamic ablation. The knowledge obtained can then be used in the preliminary design of the thermal protection system and in designing appropriate ablation experiments.

To fix the idea, we consider the steady aerodynamic ablation in the neighborhood of a two-dimensional stagnation-point of a circular-nosed body in hypersonic flow. Here the aerodynamic heating is expected to be the most intense, and yet the attendant viscous air flow is likely to be laminar. Various complicated chemical reactions including those taking place within the ablative materials are not considered in the present model for simplicity, but they may be included in future efforts. The model, which was described in detail in Ref. 1 along with an approximate analysis, should be relevant to cases where the ablation process involves melting of ablative material, for example, ablation of glassy materials studied by Hidalgo.[2] We note that the model proposed here has a similar structure to the one used by Roberts,[3] who studied the problem of ice melting in a low-speed airflow.

As was indicated in Ref. 1, an exact analysis of the model problem could be carried out by solving the conservation equations of the melt layer and the air boundary layer exactly based on the formulation of similarity solutions. In this paper, we will present such an analysis with particular emphasis on the melt layer. The equations of motion of the melt layer are first reduced to a single nonlinear ordinary differential equation for the normal component of the velocity, and the boundary conditions on the two interfaces are properly derived. The equation is then solved numerically to provide the melt-layer flowfield, including the pressure distribution. As expected, the solution depends on some parameters that must be determined by properly coupling the melt layer to the air boundary layer on one side and to the ablating solid on the other. The energy equation, which involves the velocity field, is then solved, and the temperature distribution in the melt layer is given in a simple analytical form. The shielding effect of the melt layer, thus, can be easily assessed. A procedure is outlined for solving the whole ablation problem by coupling the melt layer to the gas boundary layer and the ablating solid based on the exact solutions for the different regions of the model. To facilitate the actual computation, integral solutions are also obtained for the boundary-layer flow and the melt-layer flow, and they are used in the coupling. Explicit results for the ablation rate and melt-layer thickness, among other ablation parameters, are thus obtained in terms of the given flow and material properties for some representative cases of aerodynamic ablation.

II. Analysis

The flow configuration and the model structure are shown, respectively, in Figs. 1 and 2, and their description may be found in Ref. 1. In brief, the model consists of an inviscid hypersonic flow that drives the flow in the air boundary layer (region 1). A melt layer, region 2, that is made up of the molten solid forms underneath the boundary layer, and the two-dimensional motion of the melt allows part of the thermal energy to be convected away from the stagnation-point, thus providing the so-called shielding effect to the ablating solid. The melt layer connects to the ablating solid, region 3, through the interface, that is, the ablating front, where an additional amount of heat energy in the melt is consumed as the latent heat of ablation, resulting in a further reduction of the heat flux entering into the solid structure.

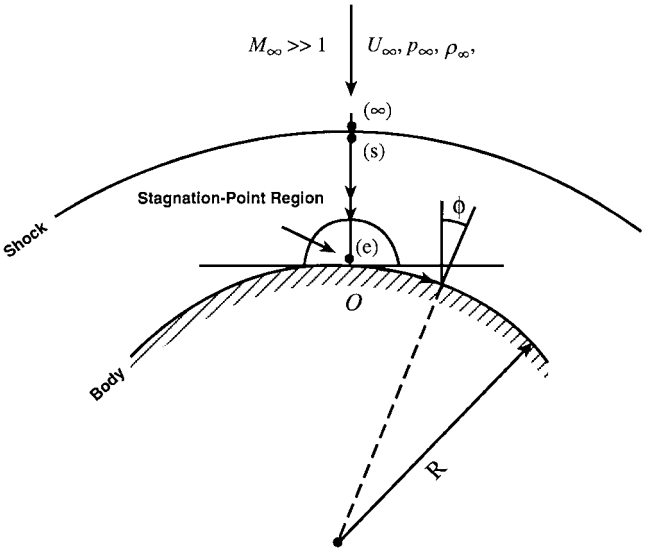

Fig. 1 Flow configuration and inviscid flowfield.

In the following analysis, the coordinate system is fixed with the ablation front, which is receding with an unknown, but constant speed W_m. In this coordinate system, the ablation front ($z = 0$) appears stationary, and the molten solid is being injected into the melt layer at a velocity equal to W_m.

A. Inviscid Flow

The inviscid flow downstream of the shock wave is first calculated, using the Newtonian theory for hypersonic flows. The surface pressure distribution obtained is used to determine the inviscid velocity gradient at the stagnation-point, and this serves as the starting point of the analysis of the model problem. Results of the inviscid flow calculation are available in Ref. 1, and they are summarized here for easy reference.

The freestream is specified by its velocity, density, and pressure, denoted, respectively, by U_∞, ρ_∞, and p_∞. For simplicity, the air is assumed to be a calorically perfect gas. The Mach number is assumed to be very large, $M_\infty^2 \gg 1$, so that the shock wave is strong and the Newtonian theory applies. In this limit, the surface pressure near the stagnation-point of the circular-nosed body of radius R is given by the following simple expression (e.g., see Refs. 4 and 5):

$$p_b(x) \cong p_{e0} - \rho_\infty u_\infty^2 x^2/R^2 \tag{1}$$

where p_{e0} is the stagnation-point pressure in the Newtonian limit. We note that $\phi = x/R \to 0$, and also $p_\infty \ll p_{e0}$ in this limit.

Note that the inviscid surface pressure as given by Eq. (1) is equal to the pressure on the air–melt interface, $p_1^*(x)$, under the boundary-layer approximation. It will be used later in coupling the flows in regions 1 and 2.

The inviscid velocity gradient at the stagnation-point $(du_e/dx)_0$ is related to the surface pressure gradient by the inviscid momentum equation and is evaluated as[1]

$$\beta_1 = \left(\frac{du_e}{dx}\right)_0 = \frac{u_\infty\sqrt{2(1+N)}}{RM_\infty} \tag{2}$$

In Eq. (2), N is the Newtonian flow parameter defined by

$$N \equiv M_\infty^2(\gamma - 1)/(\gamma + 1) = \mathcal{O}(1) \tag{3}$$

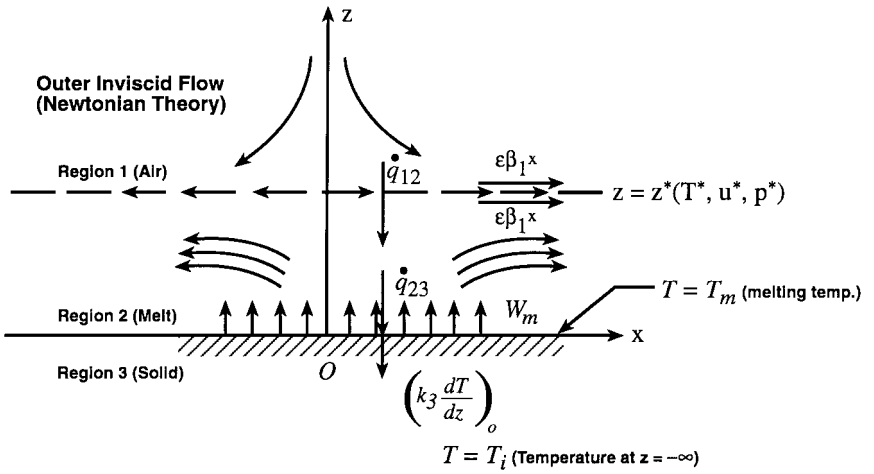

Fig. 2 Ablation model structure (coordinate system fixed on ablation front).

B. Stagnation-Point Boundary Layer

The airflow above the moving melt layer is modeled as the stagnation-point boundary layer for which similarity solutions exist. The classical formulation of the self-similar flows is slightly modified to allow for the (slow) motion of the air–melt interface, $z = z^*$, whose location is unknown in advance. Specifically, we will assume that the air velocity at the interface is $(u^*, w^*) = (\varepsilon\beta_1 x, 0)$ so that the similarity structure of the boundary layer is preserved. Here, ε is an unknown constant that must be determined as part of the solution. It measures the speed of the melt motion relative to that of the air in the boundary layer and is expected to be small.

Following Ref. 1, we will use the subscript 1 to denote conditions in this region (region 1) and the superscript $*$ to denote conditions at the air–melt interface. Modified similarity variables[3] (ξ_1, η_1) are used in the following calculations:

$$\xi_1 = \xi_1(x) = \beta_1 \rho_1^* \mu_1^* (x^2/2) \tag{4}$$

$$\eta_1 = \eta_1(x, z) = \sqrt{\frac{\beta_1}{\rho_1^* \mu_1^*}} \int_{z^*}^{z} \rho_1 \, dz \tag{5}$$

where standard notations are used. Note that $\eta_1 = 0$ at the air–melt interface.

The momentum and energy equations pertaining to the self-similar, hypersonic stagnation-point boundary layers can be reduced to the following set of coupled ordinary differential equations for $f_1'(\eta_1)$ and $g_1(\eta_1)$ (Ref. 6):

$$(C f_1'')' + f_1 f_1'' + g_1 - (f_1')^2 = 0 \tag{6}$$

$$g_1'' + (Pr_1/C) f_1 g_1' = 0 \tag{7}$$

where $f_1(\eta_1)$ is related to a stream function such that

$$u = \beta_1 x f_1'(\eta_1) \tag{8}$$

and $g_1(\eta_1)$ is the nondimensional temperature, that is,

$$T/T_e = g_1(\eta_1) \tag{9}$$

where T_e is the temperature in the external inviscid flow. The appropriate boundary conditions for f_1 and g_1 are

$$f_1(0) = 0, \qquad f_1'(0) = \varepsilon, \qquad f_1'(\infty) = 1 \tag{10a}$$

$$g_1(0) = T^*/T_e \equiv R^*(\text{unknown}), \qquad g_1(\infty) = 1 \tag{10b}$$

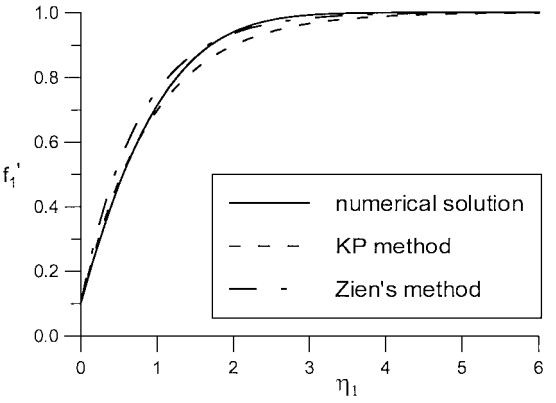

a) Velocity profile

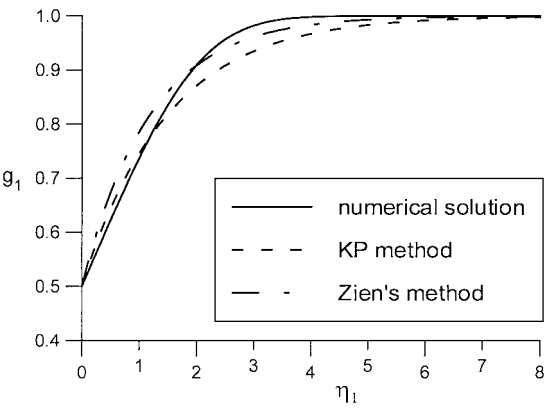

b) Temperature profile

Fig. 3 Stagnation-point boundary layer (region 1) for $\varepsilon = 0.1$ and $R^* = 0.5$.

In the preceding equations, we have used the standard viscosity–temperature relation, that is, $\rho_1 \mu_1 = C \rho_1^* \mu_1^*$, and the Prandtl number of the air Pr_1 is assumed to be constant, $Pr_1 = 0.7$.

Note that in the system of differential equations [Eqs. (6–10)] two unknown constants, ε and R^*, appear in the boundary conditions. They must be determined when the boundary-layer solutions are coupled to the melt-layer solution. The solutions of $f_1(\eta_1; \varepsilon, R^*)$ and $g_1(\eta_1; \varepsilon, R^*)$ are easily obtained numerically by a fourth-order Runge–Kutta shooting method for given values of (ε, R^*). Solutions of $f_1'(\eta_1)$ and $g_1(\eta_1)$ for $(\varepsilon, R^*) = (0.1, 0.5)$ and $(0.2, 0.5)$ are shown in Figs. 3 and 4, respectively. Corresponding integral solutions are also included in Figs. 3 and 4 for comparison, and they will be discussed in some detail later in Sec. IV.

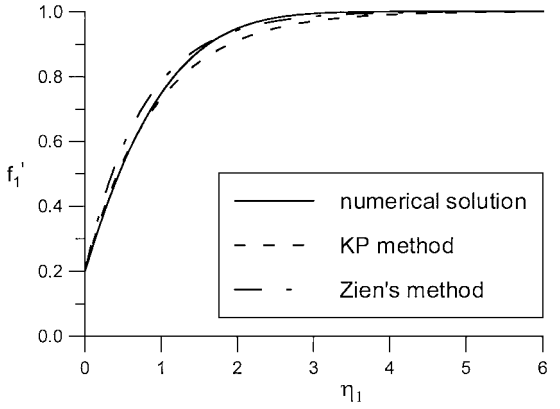

a) Velocity profile

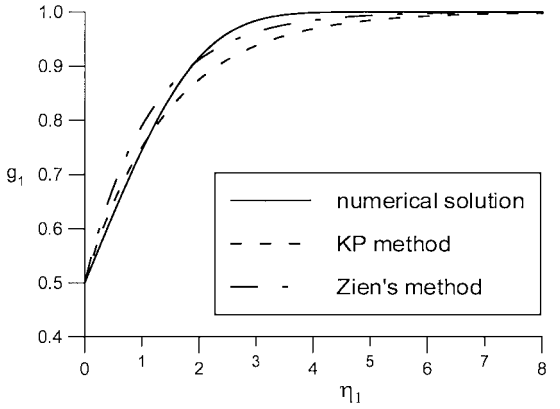

b) Temperature profile

Fig. 4 Stagnation-point boundary layer (region 1) for $\varepsilon = 0.2$ and $R^* = 0.5$.

Important quantities to be used in the coupling include the shear stress and the heat flux at $z = z^*$. They are given, respectively, in the following for later use:

$$\tau_1^* = \sqrt{\rho_1^* \mu_1^* \beta_1}\, \beta_1 x f_1''(0) \tag{11a}$$

$$(\dot{q}_{12})_1 = \left(k_1^* / c_{p1}\right)\sqrt{\left(\beta_1 \rho_1^* / \mu_1^*\right)}\, H_1 g_1'(0) \tag{11b}$$

where H_1 is the total enthalpy of the external inviscid stream. Finally, the pressure is the same as that of the inviscid surface pressure given by Eq. (1) in the boundary-layer approximation:

$$p_1(x) = p_b(x) \tag{11c}$$

To facilitate the coupling process, some approximate solutions of f_1 and g_1 that will give explicit dependence of the solutions on the parameters ε and R^* may be desirable. Therefore, integral solutions of the Eqs. (7–10) will be obtained and discussed in Sec. IV.

C. Melt Layer

The flow in this region is assumed to be viscous and incompressible, and the conservation equations for mass, momentum, and energy are, respectively, given in the following:

$$\frac{\partial u}{\partial x} + \frac{\partial w}{\partial z} = 0 \tag{12}$$

$$u\frac{\partial u}{\partial x} + w\frac{\partial u}{\partial z} = -\frac{1}{\rho_2}\frac{\partial p_2}{\partial x} + \frac{1}{\rho_2}\left(\frac{\partial}{\partial x}\mu_2\frac{\partial}{\partial x} + \frac{\partial}{\partial z}\mu_2\frac{\partial}{\partial z}\right)\mu \tag{13}$$

$$u\frac{\partial w}{\partial x} + w\frac{\partial w}{\partial z} = -\frac{1}{\rho_2}\frac{\partial p_2}{\partial z} + \frac{1}{\rho_2}\left(\frac{\partial}{\partial x}\mu_2\frac{\partial}{\partial x} + \frac{\partial}{\partial z}\mu_2\frac{\partial}{\partial z}\right)w \tag{14}$$

$$\rho_2 C_{p2}\left(u\frac{\partial}{\partial x} + w\frac{\partial}{\partial z}\right)T = \left(\frac{\partial}{\partial x}k_2\frac{\partial}{\partial x} + \frac{\partial}{\partial z}k_2\frac{\partial}{\partial z}\right)T \tag{15}$$

where the notations are standard and the subscript 2 is used to denote quantities in this region. The boundary conditions are

$$z = 0: \qquad u = 0, \qquad w = W_m, \qquad T = T_m \tag{16}$$

$$z = z^*: \qquad u = \varepsilon\beta_1 x, \qquad w = 0, \qquad T = T^* \tag{17}$$

where T_m is the constant melting temperature of the solid, T^* is equal to the air temperature at the air–melt interface [Eq. (10b)], and W_m is the unknown ablation speed. Note that the boundary conditions imply the continuity of $(\boldsymbol{u}, \boldsymbol{w}, T)$ across the air–melt interface. Also, we have made the approximation that the density of the melt is the same as that of the solid. For glassy materials, which are very viscous, the momentum equations can be simplified somewhat, but the viscous dissipation term in the energy equation may become important.

1. *Continuity Equation*

In view of the boundary conditions on $(\boldsymbol{u}, \boldsymbol{w})$, Eqs. (16) and (17), and the matching requirements with the similarity solution in the air boundary layer, we seek the solutions of $(\boldsymbol{u}, \boldsymbol{w})$ in the following forms:

$$\boldsymbol{u} = u^* F_1(\eta_2) \tag{18}$$

$$\boldsymbol{w} = W_m F_2(\eta_2) \tag{19}$$

In the preceding equations, u^* is the airspeed at the interface,

$$u^* = \varepsilon\beta_1 x \tag{20}$$

and η_2 is the similarity variable in region 2, defined as

$$\eta_2 = z/z^* \tag{21}$$

where z^* is the unknown melt-layer thickness.

Integrating the continuity equation [Eq. (12)] across the melt layer at a fixed x and invoking the boundary condition Eqs. (16) and (17), we have

$$W_m = \varepsilon\beta_1 z^* \int_0^1 F_1 \, \mathrm{d}\eta_2 \tag{22}$$

It is clear from Eq. (22) that $z^* = \text{const}$ (unknown) is compatible with the formulation of the similarity solutions for the case of steady ablation with $W_m = \text{const}$. Physically, this means that the molten solid moves with increasing speed away from the stagnation-point ($\sim\varepsilon\beta_1 x$) to accommodate the mass increase in the melt layer due to the injection of molten solid at $z = 0$, so that the melt layer maintains a constant thickness.

Thus, the continuity equation gives a relationship between F_1 and F_2,

$$F_2'(\eta_2) = -K_1 F_1(\eta_2) \tag{23}$$

where the constant parameter K_1 is defined as

$$K_1 = \varepsilon\beta_1 z^*/W_m = \text{const} \tag{24}$$

Note that the case of a linear profile for F_1 used by Zien[1] corresponds to a special case here with $K_1 = 2$.

2. Momentum Equations

In this section, we will derive an ordinary differential equation for $F_2(\eta_2)$ from the momentum equations, and the pressure distribution in the melt region will then be expressed explicitly in terms of F_2.

Substituting Eqs. (18), (19), (23), and (24) into Eqs. (13) and (14), we obtain, respectively, the following equations for the pressure gradients:

$$-\frac{\partial \tilde{p}_2}{\partial \tilde{x}} = \tilde{x}\left[(F_2')^2 - F_2F_2'' + \frac{1}{K_2}F_2'''\right] \tag{25}$$

$$-\frac{\partial \tilde{p}_2}{\partial \eta_2} = \left(F_2F_2' - \frac{1}{K_2}F_2''\right) \tag{26}$$

In the preceding equations, nondimensional quantities are used. The dimensionless pressure $\tilde{p}_2$ is introduced as

$$\tilde{p}_2 \equiv p_2/\rho_2 W_m^2 \tag{27}$$

$$\tilde{x} \equiv x/z^* \tag{28}$$

We have now introduced another dimensionless parameter K_2, defined as

$$K_2 \equiv W_m z^* \Big/ \bar{\nu}_2 \tag{29}$$

where

$$\bar{\nu}_2 \equiv \bar{\mu}_2/\rho_2 \tag{30}$$

is an average kinematic viscosity of the melt in the melt layer. It is used in the analysis strictly for simplicity. Note that K_2 so defined is a Reynolds number for the melt-layer flow under consideration.

Equation (26) gives the following equation for

$$\frac{\partial}{\partial \tilde{x}}\frac{\partial \tilde{p}_2}{\partial \eta_2} = 0 \tag{31}$$

that, when combined with Eq. (25), yields an ordinary differential equation for $F_2(\eta_2)$ as

$$\frac{\mathrm{d}}{\mathrm{d}\eta_2}\left[(F_2')^2 - F_2F_2'' + \frac{1}{K_2}F_2'''\right] = 0 \tag{32}$$

Equation (32) gives

$$(F_2')^2 - F_2F_2'' + (1/K_2)F_2''' = \tilde{c} \tag{33}$$

where $\tilde{c}$ is a constant. Its value can be determined by evaluating it at $\eta_2 = 1$, that is,

$$\tilde{c} = K_1^2 + (1/K_2)F_2'''(1) \tag{33a}$$

The following fourth-order, nonlinear ordinary differential equation for $F_2(\eta_2)$ is easily derived from Eq. (32):

$$F_2'''' + K_2(F_2'F_2'' - F_2F_2''') = 0 \tag{34}$$

The boundary conditions for Eq. (34) can easily be derived from Eqs. (16), (17), and (23) as

$$F_2(0) = 1, \qquad F_2(1) = 0, \qquad F_2'(0) = 0, \qquad F_2'(1) = -K_1 \tag{35}$$

Equations (34) and (35) determine the solution of the velocity $(\boldsymbol{u}, \boldsymbol{w})$ in the melt-layer region for a given set of values for (K_1, K_2). They are easily solved numerically by a fourth-order Runge–Kutta shooting method, and Eq. (33) can be used as a check point for the numerical solutions. It is noted that the dynamics in the melt layer is completely determined by the two parameters K_1 and K_2. These parameters are of course to be determined by properly coupling the melt layer to the air boundary layer and the solid body.

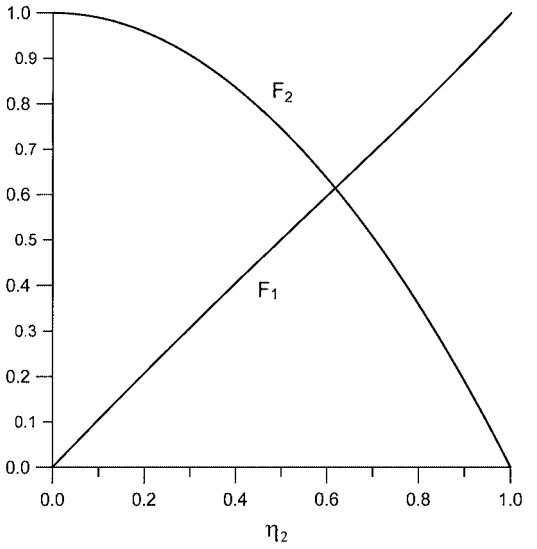

Fig. 5 Velocity profiles in the melt layer (region 2); numerical solution $(K_1, K_2) = (2, 1)$: normal velocity $F_2(\eta_2)$ and tangential velocity $F_1(\eta_2)$.

For the time being, we will write formally the solution as

$$F_2 = F_2(\eta_2;\, K_1,\, K_2) \tag{36}$$

The corresponding solution for F_1 follows from Eq. (23) and is written as

$$F_1 = F_1(\eta_2;\, K_1,\, K_2) \tag{37}$$

Solutions for the case $(K_1, K_2) = (2, 1)$ are shown in Fig. 5, which gives the velocity profiles $(\boldsymbol{u}, \boldsymbol{w})$.

Equation (31) gives the following general form of the solution for the pressure field:

$$\tilde{p}_2(\tilde{x}, \eta_2) = \tilde{A}(\tilde{x}) + \tilde{B}(\eta_2) \tag{38}$$

We note the interesting result that the pressure gradient in one direction is independent of the other.

Substituting Eq. (38) into Eqs. (25) and (26) and solving for $\tilde{A}$ and $\tilde{B}$, we obtain the following solution for the pressure field:

$$\tilde{p}_2(\tilde{x}, \eta_2) = \left(p_{e0}/\rho_2 W_m^2\right) - \tfrac{1}{2}F_2^2(\eta_2) + (1/K_2)[K_1 + F_2'(\eta_2)] - \tfrac{1}{2}\tilde{c}\tilde{x}^2 \tag{39}$$

Note that, in deriving this result, we have used the following relation:

$$\tilde{A}(0) + \tilde{B}(1) = \tilde{p}_2(0, 1) = p_{e0}/\rho_2 W_m^2 \tag{40}$$

Note that the approximate pressure field given in Ref. 1 has the form as the exact solution, that is, Eq. (38).

At the air–melt interface, we have

$$p_2^* = p_{e0} - \tfrac{1}{2}\tilde{c}\left(1\Big/K_1^2\right)\rho_2\varepsilon^2\beta_1^2x^2 \tag{41}$$

Note that the physically realistic solution of the pressure requires that $p_2^* < p_{e0}$ for $|x| > 0$. Therefore, we must have $\tilde{c} > 0$. Equation (33a) then gives a constraint on $F_2'''(1)$:

$$K_1^2 + \frac{F_2'''(1)}{K_2} > 0 \tag{42}$$

Finally, the shear stress at the air–melt interface is given by

$$\tau_2^* = -\mu_2^*\varepsilon\beta_1\frac{F_2''(1)}{K_1}\frac{x}{z^*} \tag{43}$$

where Eq. (23) has been used.

3. Energy Equation

The solution of the energy equation is the same as that given in Ref. 1, except that the exact velocity field $(\boldsymbol{u}, \boldsymbol{w})$ as given by the solution $F_2(\eta_2)$ is now used in the solution of the energy equation. We rewrite the energy equation [Eq. (15)] as

$$\rho_2 c_{p2}\left(\frac{\partial}{\partial x}uT + \frac{\partial}{\partial z}wT\right) = \left(\frac{\partial}{\partial x}k_2\frac{\partial}{\partial x} + \frac{\partial}{\partial z}k_2\frac{\partial}{\partial z}\right)T \tag{44}$$

In this form, the effect of the convection in the melt layer on the heat fluxes in and out of the region can be made apparent by simply integrating the equation across the melt layer. We introduce a nondimensional temperature Θ_2, defined as

$$\Theta_2(\eta_2) \equiv (T - T_m)\Big/\left(T^* - T_m\right) = G_2(\eta_2) \tag{45}$$

where T_m is the melting temperature of the solid and it is also the temperature at the ablation surface. Next, as in Ref. 1, we assume that Θ_2 is only weakly dependent on x, that is, the thin melt-layer approximation. Then integrating Eq. (44) across the entire melt layer and using the appropriate boundary conditions on $\boldsymbol{u}$, $\boldsymbol{w}$, and T as given by Eqs. (16) and (17), we obtain

$$(\dot{q}_{12})_2 - (\dot{q}_{23})_2 = \rho_2 c_{p2}\left(T^* - T_m\right)\varepsilon\beta_1 z^* \int_0^1 F_1\Theta_2\,\mathrm{d}\eta_2 \tag{46}$$

In Eq. (46), $(\dot{q}_{12})_2$ and $(\dot{q}_{23})_2$ are, respectively, the heat fluxes into and out of the melt layer (see Fig. 2):

$$(\dot{q}_{12})_2 = k_2^*\left(\frac{\partial T}{\partial z}\right)_{z^*} \tag{47}$$

$$(\dot{q}_{23})_2 = k_{2m}\left(\frac{\partial T}{\partial z}\right)_0 \tag{48}$$

where the subscript m denotes conditions at the ablation front, $z = 0$, and the superscript $*$ denotes conditions at $z = z^*$, as before.

Equation (46) states that the convection current accounts for the reduction of heat flow in the normal direction, and the effect of the melt layer as a heat shield is, thus, apparent.

For simplicity, we will use an average thermal conductivity $\bar{k}_2$ for the melt to account for the effect of significant temperature variations anticipated in the melt layer. Thus, we write Eq. (15) in nondimensional form as follows:

$$KF_2(\eta_2)\frac{\mathrm{d}G_2}{\mathrm{d}\eta_2} = \frac{\mathrm{d}^2G_2}{\mathrm{d}\eta_2^2} \tag{49}$$

where another dimensionless parameter K is introduced, and it is an effective Peclet number of the melt defined by

$$K \equiv W_m z^*\Big/\bar{\alpha}_2 \tag{50}$$

with $\bar{\alpha}_2$ denoting the effective thermal diffusivity, $\bar{\alpha}_2 = \bar{k}_2/\rho_2 c_{p2}$. The boundary conditions for Eq. (49) are

$$G_2(0) = 0, \qquad G_2(1) = 1 \tag{51}$$

The solution of $G_2(\eta_2)$ is easily obtained as

$$G_2(\eta_2) = I(\eta_2)/I(1) \tag{52}$$

where

$$I(\eta_2) = \int_0^{\eta_2} \exp\left(K\int_0^{\eta_2} F_2\,\mathrm{d}\eta_2\right)\mathrm{d}\eta_2 \tag{53a}$$

$$I(1) = \int_0^{1} \exp\left(K\int_0^{\eta_2} F_2\,\mathrm{d}\eta_2\right)\mathrm{d}\eta_2 \tag{53b}$$

It then follows that

$$(\dot{q}_{12})_2 = \left[k_2^*\left(T^* - T_m\right)\Big/z^*\right][E(1)/I(1)] \tag{54a}$$

$$(\dot{q}_{23})_2 = \left[k_{2m}\left(T^* - T_m\right)\Big/z^*\right][1/I(1)] \tag{54b}$$

where

$$E(1) = \exp\left(K\int_0^1 F_2\,\mathrm{d}\eta_2\right) \tag{54c}$$

The shielding factor r defined as

$$r = (\dot{q}_{23})_2/(\dot{q}_{12})_2 \tag{55a}$$

is given by

$$r = \left(k_{2m}\Big/k_2^*\right)[1/E(1)] = r\left[K,\ K_1,\ K_2,\ \left(k_{2m}\Big/k_2^*\right)\right] \tag{55b}$$

In the derivation of this result, the ratio k_{2m}/k_2^* appears naturally, although in the solution of the energy equation, some average value of the thermal conductivity $\bar{k}_2$ was used. Note that the result for r could also be derived directly from Eq. (46). It is clear from Eq. (55b) that $r < 1$, as expected. Also, the result of r given in Ref. 1 can be recovered as a special case of the present general result where the approximate velocity profiles, $F_1 = \eta_2$ and $F_2 = 1 - \eta_2^2$, were used. Results of r for the case of $(K, K_1, K_2) = (5, K_1, 1)$ are shown in Fig. 6, corresponding to $Pr_2 = 5$. It is assumed that $k_2^* = k_{2m}$ for simplicity. From Eqs. (24) and (29), we have

$$K_1 K_2 = \varepsilon\beta_1(z^*)^2\Big/\bar{\nu}_2 \tag{56}$$

Therefore, for a given K_2, the parameter $K_1 \sim \varepsilon(z^*)^2$. It is seen in Fig. 6 that r decreases as ε or z^* increases, which is intuitively correct. It is also clear that the melt layer provides a better heat shield to the solid if the molten ablative material has lower thermal diffusivity, that is, higher Prandtl number.

Of course, K_1 and K_2 are functions of the flow parameters in the melt region, and they must be related to those of the air and solid region through coupling to complete the solution of the model ablation problem under consideration.

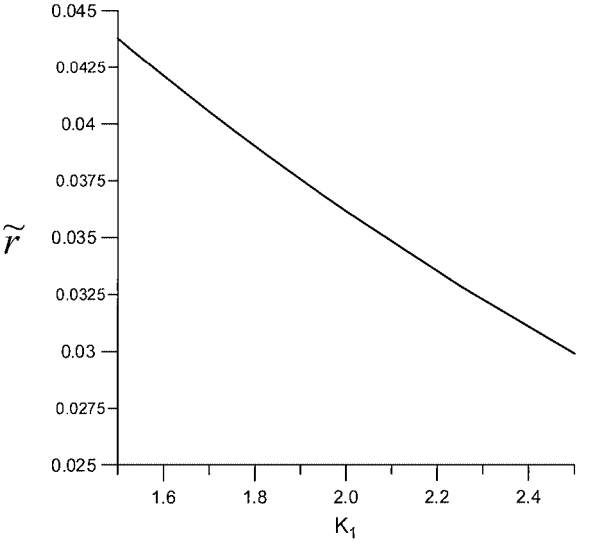

Fig. 6 Shielding factor $\tilde{r} = \tilde{r}(K_1)$: $K_2 = 1$, $Pr_2 = 5.0$ [note: $\tilde{r} \equiv (k_2^*/k_{2m})r = (k_2^*/k_{2m})(\dot{q}_{23})_2/(\dot{q}_{12})_2$].

D. Ablating Solid

As in Ref. 1, a one-dimensional heat conduction model is used for the heat transfer in the ablating solid. In the coordinate system used in the present analysis, the heat conduction appears steady. The Galilean transformation is used to transform the transient conduction equation to the following steady-state equation with the boundary conditions:

$$\rho_3 c_3 W_m \frac{\mathrm{d}T}{\mathrm{d}z} = \frac{\mathrm{d}}{\mathrm{d}z}\left(k_3 \frac{\mathrm{d}T}{\mathrm{d}z}\right)$$

$$T(0) = T_m, \quad T(-\infty) = T_i \text{ (given)} \tag{57}$$

where T_i is the temperature of the solid far away from the ablating front.

The solution for the temperature is easily obtained as[1]

$$\Theta_3 = (T - T_i)/(T_m - T_i) = \exp(W_m z/\bar{\alpha}_3) \tag{58}$$

where, as in Sec. II.C.3, an average value of thermal conductivity, $\bar{k}_3$, is used to simplify the result, and the thermal diffusivity of the solid, $\bar{\alpha}_3$, is thus assumed constant.

At the ablation front, $z = 0$, the heat balance requires that

$$(\dot{q}_{23})_2 = \left(k_3 \frac{\mathrm{d}T}{\mathrm{d}z}\right)_0 + \rho_3 Q_L W_m \tag{59}$$

where Q_L is the latent heat of ablation per unit mass of the solid.

It is clear from Eq. (59) that the ablation process serves as an additional heat shield for the structure, as it consumes part of the heat flux coming from the melt layer, thus reducing further the heat flux into the solid. Upon substitution of the solution of the temperature, Eq. (58), into Eq. (59), we have

$$(\dot{q}_{23})_2 = c_3 \rho_3 W_m (T_m - T_i)(1 + \upsilon) \tag{60}$$

where $\upsilon \equiv Q_L/c_3(T_m - T_i)$ is an ablation parameter (e.g., see Ref. 7).

III. Coupling

The solutions for different regions for the model, presented in Sec. II, must be coupled to form a complete solution for the physical problem of ablation under consideration. The coupling is accomplished by appropriate boundary conditions on the interfaces.

A. Air-Melt Interface ($z = z^*$)

The interface boundary conditions here are continuity of velocity, $(\boldsymbol{u}, \boldsymbol{w})$, and temperature, which have already been incorporated into the formulation for the problem. In addition, the following boundary conditions are required:

1) Continuity of heat flux

$$(\dot{q}_{12})_1 = (\dot{q}_{12})_2 \tag{61}$$

because no phase changes or chemical reactions on the interface are considered in the present model.

2) Continuity of normal stress is required. Because the viscous normal stress ($\sim \mu_2 \partial w/\partial z$) is expected to be small compared to the pressure in the hypersonic environments considered here, the pressure is continuous across the interface:

$$p_1(x) = p_2^*(x) \tag{62}$$

Using Eqs. (11c) and (41) for $p_1(x)$ and $p_1^*(x)$, respectively, we see that the pressure matching is possible and that the parameter ε is related to the flow parameters of the melt layer, $\tilde{c}$ and K_1 by the following equation:

$$\varepsilon = M_\infty \left(\frac{\rho_\infty}{\rho_2} \frac{K_1^2}{\tilde{c}} \frac{1}{1+N}\right)^{\frac{1}{2}} \tag{63}$$

after Eq. (2) is used for β_1. In a typical hypersonic ablation case where $M_\infty = \mathcal{O}(10)$ and $\rho_\infty/\rho_2 = \mathcal{O}(10^{-4})$, Eq. (63) gives $\varepsilon = \mathcal{O}(10^{-1})$, which is indeed small.

3) Continuity of shear stress is required. Here, we require $\tau_1^* = \tau_2^*$. Equations (11a) and (43) then give the following relation between the melt-layer thickness and the flow parameters in the air boundary layer:

$$z^* = -\frac{\varepsilon F_2''(1)}{K_1} \frac{\mu_2^*}{\mu_1^*} \sqrt{\frac{\mu_1^*}{\rho_1^* \beta_1}} \frac{1}{f_1''(0)} \tag{64}$$

B. Melt-Solid Interface ($z = 0$)

The heat balance equation [Eq. (59)] couples the melt region to the ablating solid, and the continuity of velocity at the interface, $(\boldsymbol{u}, \boldsymbol{w}) = (0, W_m)$ is already accounted for in the formulation of the flow problem in region 2.

C. Summary of the Results of Coupling

Combining Eqs. (11b), (54a), and (61), we get

$$\frac{k_1^*}{c_{p1}} \left(\frac{\beta_1 \rho_1^*}{\mu_1^*}\right)^{\frac{1}{2}} H_1 g_1'(0) = \frac{k_2^*(T^* - T_m)}{z^*} \frac{E(1)}{I(1)} \tag{65}$$

Combining Eqs. (54b) and (60), we get

$$\left(k_{2m}/z^*\right)\left[\left(T^* - T_m\right)/I(1)\right] = c_3 \rho_3 W_m (T_m - T_i)(1 + \upsilon) \tag{66}$$

Equations (24), (29), (33), and (63–66) form a system of seven equations for the solutions of the seven unknowns, ε, R^*, K_1, K_2, $\tilde{c}$, z^*, and W_m, in terms of the given conditions of the freestream and the material properties involved. However, the actual system is larger because we have quantities such as $f_1''(0)$ and $g_1'(0)$ that are functions of ε and R^*, and their functional dependence is through the differential equations, that is, Eqs. (6–10). A similar situation applies to quantities $F_2''(1)$ and $F_2'''(1)$, whose functional dependence on K_1 and K_2 is through the differential equations [Eqs. (34) and (35)]. The implicit functional dependence necessitates an iterative procedure that involves solving differential equations in each iteration of the actual computation. Parametric studies, which are necessary in the design process, would become impractical.

In the next section we will present integral solutions for the air boundary layer and the melt layer. These solutions, though approximate, exhibit explicit dependence on the parameters ε, R^*, K_1, and K_2, and their use in the solution of the coupled system of equations greatly facilitates the actual computation. Furthermore, the approximate solutions thus obtained can be used as a starting point in the iterative process of solving the more exact system that involves numerical solutions of some nonlinear differential equations for the boundary-value type, that is, Eqs. (6–10), (34), and (35).

D. Length and Velocity Scales

To present and discuss results in a nondimensional form, we will first introduce the following length and velocity scales:

$$\ell = \left(\nu_1^*/\beta_1\right)^{\frac{1}{2}} \tag{67a}$$

$$V = \left(\beta_1 \nu_1^*\right)^{\frac{1}{2}} \tag{67b}$$

where ν_1^* is the kinematic viscosity of air at $T = T^*$. Note that l is a measure of the thickness of the air boundary layer of region 1. Using l and V, we define dimensionless z^* and W_m as follows:

$$\overline{z^*} = z^*/\ell \tag{68a}$$

$$\overline{W_m} = W_m/V \tag{68b}$$

The system of equations listed in Sec. III.C can be easily cast into dimensionless form using $\overline{z^*}$ and $\overline{W_m}$.

Let us consider the case of reentry of Apollo 11 discussed in Ref. 4. Here we have $M_\infty = 32$ and $T_\infty = 280$ K. We assume $\varepsilon = 0.1$, $R = 0.5$ m, $\gamma = 1.02$, and $T^* = 2300$ K. Under these conditions, we have $\nu_1^* = 5 \times 10^{-4}$ m^2/s (e.g., see Eckert and Drake[8]), $N = 10$, $u_\infty = 9$ km/s and $\beta_1 = 2700$ s^{-1}. Therefore, $l \cong 0.4 \times 10^{-3}$ m and $V \cong 1.2$ m/s.

IV. Integral Solutions

In this section, we will present some integral solutions for the air boundary-layer flows (region 1) and the melt-layer flows (region 2). These approximate solutions will be used later in the coupling, and results will be presented for some selected cases of the model problem. Only the results of application of the Kármán–Pohlhausen (KP) integral method will be used in the coupling, although some results of the application of the Zien's modified KP method (e.g., see Ref. 9) to the boundary-layer calculations will be presented to indicate the potential of the integral solutions for further improvements. Detailed results of Zien's method for the ablation calculations will appear in a later paper.

A. Air Boundary Layer

First we assume the following forms for the solutions of f_1 and g_1, that satisfy the boundary conditions [Eqs. (10a) and (10b)]:

$$f_1(\eta_1) = \eta_1 + [(1-\varepsilon)/\alpha_1](e^{-\alpha_1\eta_1} - 1), \qquad \alpha_1 > 0 \quad (69a)$$

$$g_1(\eta_1) = 1 - (1-R^*)e^{-\alpha_2\eta_1}, \qquad \alpha_2 > 0 \quad (69b)$$

where α_1 and α_2 are two profile parameters to be determined.

The quantities of particular interest to our problem, $f_1''(0)$ and $g_1'(0)$, are given as functions of α_1, α_2, R^*, and ε:

$$f_1''(0) = \alpha_1(1-\varepsilon) \quad (70a)$$

$$g_1'(0) = \alpha_2(1-R^*) \quad (70b)$$

Note that $Pr_1 = 0.7$ and $C = 1$ will be used in all of the calculations.

Integrating Eqs. (6) and (7) and substituting Eqs. (69a and 69b) for f_1 and g_1, we have

$$C\alpha_1^2\alpha_2(1-\varepsilon) - \alpha_2(1-\varepsilon)(2+\varepsilon) + \alpha_1(1-R) = 0 \quad (70c)$$

$$Pr_1(\alpha_1 + \alpha_2\varepsilon) - C\alpha_2^2(\alpha_1 + \alpha_2) = 0 \quad (71)$$

For a given set of values of (ε, R^*), the given simultaneous algebraic equations determine α_1 and α_2. The results are easily obtained, and Figs. 7a and 7b show the solutions of $f_1''(0; \varepsilon, R^*)$ and $g_1'(0; \varepsilon, R^*)$, which are the quantities required in the coupling. Solutions by Zien's integral method (the η_1-moment scheme[9]) are also included in the comparison. Note that, although the KP solutions for the velocity and temperature are reasonably accurate, the KP solutions for $f_1''(0)$ and $g_1'(0)$ are not as accurate as Zien's solutions. This indicates that Zien's method will give improved results for the coupled problem. However, for the present purpose, we will proceed with the KP method of solutions.

B. Melt Layer

Returning to Eqs. (34) and (35) we will now apply the KP integral method of their solution. First, we assume a polynomial form of the solution as

$$F_2(\eta_2) = 1 + (-3 + K_1 + \alpha_3)\eta_2^2 + (2 - K_1 - 2\alpha_3)\eta_2^3 + \alpha_3\eta_2^4 \quad (72)$$

which satisfies the boundary conditions, Eq. (35). The profile parameter α_3 will be determined by the KP method.

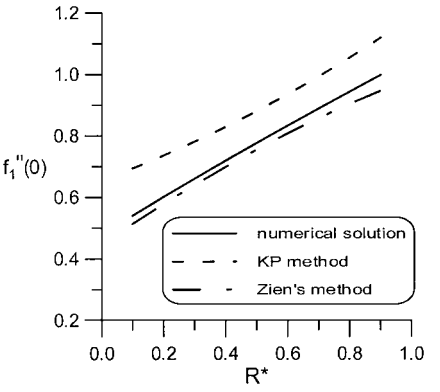

a) $f_1''(0; \varepsilon, R^*)$: region 1, $\varepsilon = 0.2$

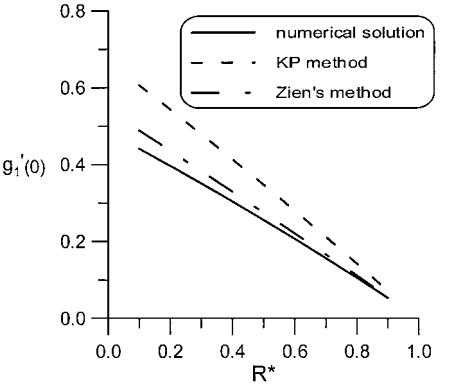

b) $g_1'(0; \varepsilon, R^*)$: region 1, $\varepsilon = 0.2$

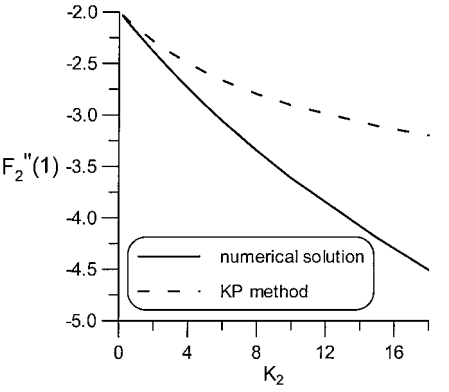

c) $F_2'(1; K_1, K_2)$: region 2, $K_1 = 2$

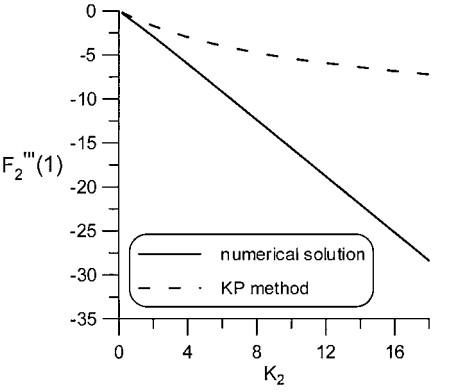

d) $F_2''(1; K_1 K_2)$: region 2, $K_1 = 2$

Fig. 7 Integral solutions (regions 1 and 2).

Integrating Eq. (34) across the melt layer and substituting Eq. (72) for F_2 and taking its derivatives as they appear in the integrated equation, we arrive at an algebraic equation that gives the solution for α_3:

$$\alpha_3 = \frac{K_2}{2}\frac{6 - 2K_1 - K_1^2}{12 + K_2} \tag{73}$$

The quantities of particular interest to the coupling of solutions are (see Sec. III.C)

$$F_2''(1) = 2(3 - 2K_1 + \alpha_3) \tag{74a}$$

$$F_2'''(1) = 6(2 - K_1 + 2\alpha_3) \tag{74b}$$

Figures 7c and 7d show, respectively, the results of $F_2''(1)$ and $F_2'''(1)$ as functions of K_2 for $K_1 = 2$. It is seen that the KP solutions become less accurate as K_2 increases. Here the ideas used in Zien's integral method[7,9] may provide some improvement to the integral solutions.

Note also that in the integral solution discussed here, the constant $\tilde{c}$ defined in Eq. (33) is no longer a constant for all values of η_2 because the approximate solution given by Eq. (72) satisfies only the integrated form of the differential equation, not locally.

Thus, we evaluate $\tilde{c}$ by its value at $\eta_2 = 1$:

$$\tilde{c} = \tilde{c}(\eta_2 = 1) = K_1^2 + 6(2 - K_1 + 2\alpha_3)/K_2 \tag{75}$$

and it is obvious that $\tilde{c}(\eta_2 = 1) = \tilde{c}(\eta_2 = 0)$ in the integral solution.

The solution of the energy equation remains formally the same as that presented in Sec. II.C.3, except that $F_2(\eta_2)$ as given by Eq. (72) will be used in the solution of G_2 and the corresponding expressions for $(\dot{q}_{12})_2$ and $(\dot{q}_{23})_2$.

Note that we will still use the exact solution, that is, Eq. (58), for the temperature distribution in the ablating solid (region 3).

C. Coupling

The coupling of the solutions in the three different regions still follows the same boundary conditions as used in Sec. III, but the system of the resulting equations for the solution of the whole ablation problem will be different. Only algebraic equations will be involved in the solution of the problem, now that the explicit and analytical solutions for the air boundary layer and the melt layer are available to replace the numerical solutions of the original differential equations.

In terms of the integral solutions, Eqs. (64–66) may be rewritten in the following dimensionless forms:

$$\overline{z^*} = -\frac{2\varepsilon(3 + \alpha_3 - 2K_1)}{\alpha_1(1 - \varepsilon)K_1}\frac{\mu_2^*}{\mu_1^*} \tag{76}$$

$$\overline{z^*}\alpha_2(1 - R^*) = \left(k_2^*/k_1^*\right)A[E(1)/I(1)] \tag{77}$$

$$B = \frac{c_3\rho_3 v_1^*}{k_{2m}}\overline{W_m}\,\overline{z^*}I(1) \tag{78}$$

where

$$A = \left(T^* - T_m\right)/T_{e0} \tag{79}$$

$$B = \left[\left(T^* - T_m\right)/(T_m - T_i)\right][1/(1 + \upsilon)] \tag{80}$$

The system of 10 simultaneous algebraic equations, that is, Eqs. (70c), (71), (73), (75), (63), (24), (29), and (76–78) are to be solved for the 10 unknowns of the problem: α_1, α_2, α_3, ε, R^*, $\tilde{c}$, K_1, K_2, $\overline{z^*}$, and $\overline{W_m}$.

The solution procedure we propose is to assume a set of values for (ε, R^*) and use the preceding system of equations to determine the parameters A and B.

For a given set of values of M_∞, ρ_∞/ρ_2, and N, we rewrite Eq. (63) as

$$\varepsilon^2 = m\left(K_1^2/\tilde{c}\right) \tag{81}$$

where

$$m = M_\infty^2(\rho_\infty/\rho_2)[1/(1 + N)] \tag{82}$$

Equations (24) and (29) can be combined to give

$$(\overline{z^*})^2 = (K_1K_2/\varepsilon)\left(\bar{\nu}_2/\nu_1^*\right) \tag{83}$$

Eliminating $\overline{z^*}$ from Eqs. (76) and (83), we get

$$\frac{\varepsilon^3}{(1 - \varepsilon)^2} = \frac{K_1^3K_2}{4}\frac{\alpha_1^2N_m}{(3 + \alpha_3 - 2K_1)^2} \tag{84}$$

where

$$N_m = \left(\bar{\nu}_2/\nu_1^*\right)\left(\mu_1^*/\mu_2^*\right)^2 \tag{85}$$

is a parameter characterizing the materials considered in the model problem, for example, air/quartz.

Recall that α_1 is determined for a given set of values for (ε, R^*). Also we have $\alpha_3 = \alpha_3(K_1, K_2)$ and $\tilde{c} = \tilde{c}(K_1, K_2)$ from Eqs. (73) and (75), respectively. Equations (81) and (84) then provide solutions for K_1 and K_2 as functions of N_m and m:

$$K_1 = K_1(m, N_m), \qquad K_2 = K_2(m, N_m) \tag{86}$$

Equation (86) represents the solution of the coupled problem because it provides the melt-layer characteristics as determined by K_1 and K_2 in terms of the flow in the air boundary layer as determined by ε and R^*, for a given ablative system (i.e., given m and N_m). Solutions of K_1 and K_2 as given by Eq. (86) are shown in Fig. 8 as functions of N_m for the case where $(\varepsilon, R^*, m) = (0.2, 0.4, 0.1)$.

The main quantities of the ablation problem, $\overline{W_m}$ and $\overline{z^*}$, are then obtained from Eqs. (24) and (29) as

$$\overline{z^*} = \left[(K_1K_2/\varepsilon)\left(\bar{\nu}_2/\nu_1^*\right)\right]^{\frac{1}{2}} \tag{87}$$

$$\overline{W_m} = \left[(\varepsilon K_2/K_1)\left(\bar{\nu}_2/\nu_1^*\right)\right]^{\frac{1}{2}} \tag{88}$$

Finally, Eqs. (77) and (78) are used to evaluate A and B.

Note that this procedure constitutes an inverse approach because we determine the parameters A and B that characterize the freestream (i.e., u_∞) and the initial condition (i.e., T_i) corresponding to the assumed values ε and R^*, for a given ablative material.

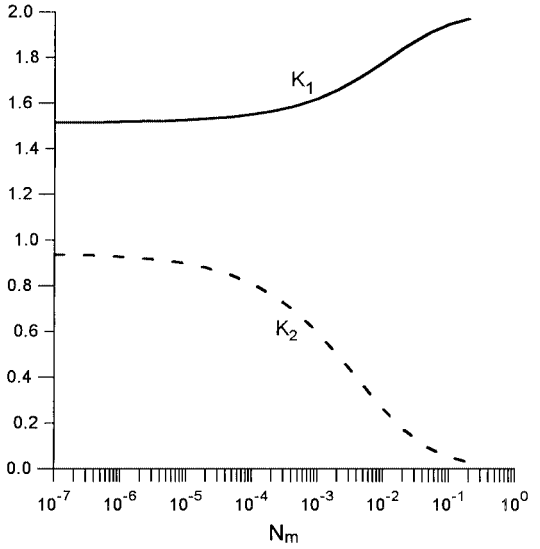

Fig. 8 Coupled solution for model ablation problem $(\varepsilon, R^*, m) = (0.2, 0.4, 0.1)$, KP (region 1)/KP (region 2); K_1 and K_2 as functions of N_m.

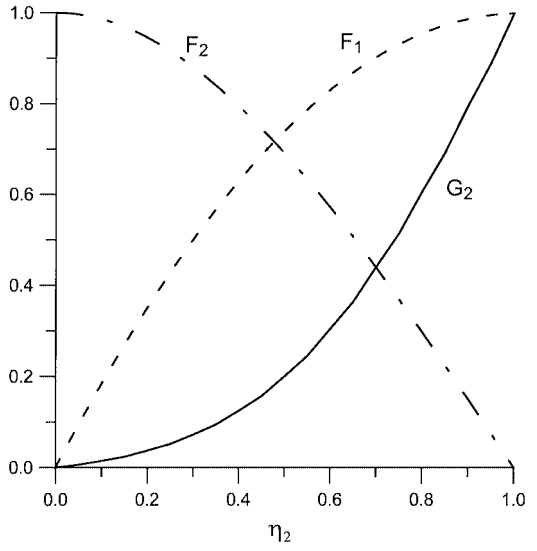

Fig. 9 Coupled solution for model ablation problem: melt-layer profiles, $(m, \varepsilon, R^*, N_m, Pr_1, Pr_2, \bar{\nu}_2/\nu_1^*) = (0.1, 0.2, 0.4, 0.75 \times 10^{-6}, 0.7, 5.0, 0.25 \times 10^{-3})$; $\alpha_1 = 1.0362$, $\alpha_2 = 0.6900$, $\alpha_3 = 4.0246$, $\overline{W_m} = 0.0055308$, and $\overline{z^*} = 0.0419135$.

D. Example

As an example of the application of the computational procedure suggested in Sec. IV.C, we consider the case where we have $(m, \varepsilon, R^*, N_m, Pr_1, Pr_2, \bar{\nu}_2/\nu_1^*) = (0.1, 0.2, 0.4, 0.75 \times 10^{-6}, 0.7, 5.0, 0.25 \times 10^{-3})$. The dimensionless constants, N_m, Pr_1, Pr_2, and $\bar{\nu}_2/\nu_1^*$, correspond roughly to the ablative system of air/lead. However, we note that lead may be a poor choice for the ablator because of its relatively high thermal diffusivity.

From the given values of ε and R^*, we first obtain the solutions for α_1 and α_2 from Eqs. (70c) and (71), that is, $(\alpha_1, \alpha_2) = (1.0362, 0.6900)$. Results in Fig. 8 are next used to determine K_1 and K_2 as $(K_1, K_2) = (1.5156, 0.9273)$. Solution for α_3 then follow from Eq. (73), $\alpha_3 = 0.0241$. Values for $\overline{z^*}$ and $\overline{W_m}$ are easily calculated from Eqs. (87) and (88), respectively, as $(\overline{z^*}, \overline{W_m}) = (0.0419, 0.00553)$. Finally, Eqs. (77) and (78) give the corresponding values for A and B, respectively, $(A, B) = (3.29 \times 10^{-3} Cp_1/Cp_2, 0.206 \times 10^{-2} \rho_3 c_3 \nu_1^*/k_{2m})$. Values A and B can be used to determine the energy level of the hypersonic stream (e.g., T_{e0}) and the temperature level of the ablating solid (e.g., T_i). Corresponding profiles in the melt layer for this example are shown in Fig. 9.

The ablation phenomenon in the thermal protection system for vertical missile launchers is another important application (e.g., see Refs. 10 and 11), but the problem is complicated by the existence of solid particles and liquid droplets of Al_2O_3 in the oncoming hot gas stream from the solid rocket exhaust. Modification of the present model for this application will be an interesting but challenging task.

V. Conclusion

The validity of the simple ablation model and its analysis presented in the paper are limited to the class of ablation problems where a melt layer forms in the process. The dynamics and heat transfer in the melt layer are analyzed, and both numerical and the KP-type of integral solutions are presented. Its effect as a heat shield to the solid structure is, thus, quantitatively assessed. The nature of the stagnation-point flow admits a class of similarity solutions that greatly simplify the analysis and computation. For some sample cases with specific values of the parameters of the model, we have successfully constructed and computed such solutions in different regions of the model and properly coupled them by using pertinent interface boundary conditions. A general proof the existence of such similarity solutions will be extremely difficult, and it is not even clear that such solutions exist over the entire domain of the parameter space of the model problem. The ultimate validation of the model and the theoretical solutions must, of course, await careful experimentation.

The assumption of an ideal gas for the flow outside the melt layer and the application of the Newtonian theory to determine the inviscid pressure field are made mainly to simplify the analysis. Real gas effects will become significant at the large Mach numbers assumed in the Newtonian theory. However, the use of the Newtonian theory is not essential to the structure of the model and its analysis. In fact, the model structure is expected to remain the same for low-speed flows also,[3] and other appropriate methods, numerical or analytical, are available for calculating the inviscid pressure field over a wide range of Mach numbers for the flow configuration of the model. We note also that the Newtonian theory is known to yield reasonably accurate pressure results for moderately high Mach numbers as well, where the real gas effects are not so important.

The model discussed does not include the effects of evaporation of the molten solid. Additional conditions of mass, momentum, and energy balance need to be considered on the air–melt interface to account for the effect of evaporation (e.g., see Ref. 2). Other effects such as pyrolysis, complex chemical reactions, and physical processes of the ablative materials are not considered in this model of simple ablation, and their inclusion will require considerable modifications.

It is believed that the accuracy of the analysis presented in this paper can be improved by using the refined integral solutions (i.e., Zien's method[7,9]) for the air boundary layer and the melt layer in the coupling. Of course, the use of the coupling procedure of Sec. III.C based on the exact solutions of all three regions, though difficult to implement, will provide the ultimate exact solution of the model ablation problem.

Acknowledgment

The research was partially supported by the U.S. Naval Surface Warfare Center, Dahlgren Division (NSWCDD) Independent Research Program, and much of the work was accomplished while T.-F. Zien was on academic leave at the National Cheng-Kung University (NCKU). We gratefully acknowledge the support and encouragement of Mary Lacey, Head of the Systems Research and Technology Department of NSWCDD, and J. J. Miau, Director of the Institute of Aeronautics and Astronautics (IAA)/NCKU. We also thank Y. N. Jeng of IAA/NCKU for some useful discussions.

References

[1]Zien, T. F., "Effects of Melt-Layer on Steady Aerodynamic Ablation in Hypersonic Flow," AIAA Paper 98-1580, April 1998.

[2]Hidalgo, H., "Ablation of Glassy Material Around Blunt Bodies of Revolution," *ARS Journal*, Vol. 30, Sept. 1960, pp. 806–814.

[3]Roberts, L., "On the Model of a Semi-Infinite Body of Ice Placed in a Hot Stream of Air," *Journal of Fluid Mechanics*, Vol. 4, 1958, pp. 505–528.

[4]Anderson, J. D., *Hypersonic and High-Temperature Gas Dynamics*, McGraw–Hill, New York, 1989, Chaps. 3 and 9.

[5]Rasmussen, M., *Hypersonic Flow*, Wiley, New York, 1994, Chap. 9.

[6]Zien, T. F., "Fundamentals of Hypersonic Aerodynamics, Part II: Advanced Topics and Real Gas Effects," Inst. of Aeronautics and Astronautics, Publ. No. 45, National Cheng-Kung Univ., Tainan, Taiwan, ROC, 1988.

[7]Zien, T. F., "Integral Solutions of Ablation Problems with Time-Dependent Heat Flux," *AIAA Journal*, Vol. 16, No. 12, 1978, pp. 1287–1295.

[8]Eckert, E. R. G., and Drake, R. M., *Heat and Mass Transfer*, McGraw–Hill, New York, 1972.

[9]Zien, T. F., "Approximate Calculations of Viscous Drag and Aerodynamic Heating," *Developments in Theoretical and Applied Mechanics*, edited by S. Y. Wang, R. M. Hackett, S. L. DeLeew, and A. M. Smith, Vol. 14, Univ. of Mississippi Press, University, MS, 1988, pp. 79–87.

[10]Lewis, D., and Anderson, L., "Effects of Melt-Layer Formation on Ablative Materials Exposed to Highly Aluminized Rocket Motor Plumes," AIAA Paper 98-0872, Jan. 1998.

[11]Cheung, F. B., Yang, B. C., Burch, R. L., and Koo, J. H., "Effect of Melt Layer Formation on Thermo-Mechanical Erosion of High-Temperature Ablative Materials," *Proceedings of 1st Pacific International Conference on Aerospace Science and Technology*, 1993, pp. 302–309.